Polymer-templated mesoporous lithium titanate microspheres for high-performance lithium batteries
– Supporting Information –

Minh Tri Nguyen,[†] Preston Sutton,[‡] Andrea Palumbo,[†] Michael G. Fischer,[†,§]

Xiao Hua,[¶] Ilja Gunkel,[*,†] and Ullrich Steiner[*,†]

[†]*Adolphe Merkle Institute, University of Fribourg, Chemin des Verdiers 4, 1700 Fribourg, Switzerland.*

[‡]*Institute for Frontier Materials, Deakin University, Burwood, VIC 3125, Australia.*

[¶]*Department of Chemical and Biological Engineering, University of Sheffield, United Kingdom.*

[§]*now at: Sensirion AG, Laubisruetistrasse 50, 8712 Staefa ZH, Switzerland*

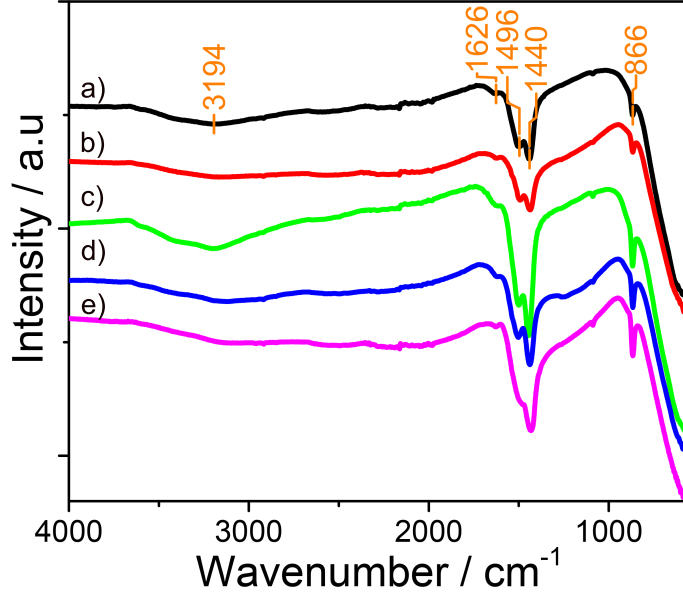E-mail: ilja.gunkel@unifr.ch; ullrich.steiner@unifr.ch

Figure S1: FTIR profiles of mesoporous LTO-A-600 (a), LTO-A-700 (b), LTO-B-600 (c), LTO-B-700 (d) and LTO-C-700 (e). The strong absorption band at approximately $3200\,\text{cm}^{-1}$ of (a,c) compared with (b,d,e) and a band at around $1630\,\text{cm}^{-1}$ correspond to the stretching and bending vibration of -OH due to adsorbed water on the surface of LTO.[1] This implies that all the samples annealed at the lower temperature are more prone to water absorption compared to the samples which were annealed at the higher temperature. The two strong vibration bands at 1496 and $1440\,\text{cm}^{-1}$ are assigned to carbonate asymmetric stretching. A weak band at $866\,\text{cm}^{-1}$ corresponds to the bending vibration of lithium carbonate Li_2CO_3.[2–4] The presence of Li_2CO_3 in all samples is due to the reaction of surface lithium with CO_2 from the air.[1,4]

Table S1: Summary of the average crystallite size[*] and porosity[**] of mesoporous LTO microspheres.

Sample	Crystallite size nm Scherrer eq.	S_{BET} m^2g^{-1} BJH	V_{pore} cm^3g^{-1} BJH	d_{pore} nm BJH
LTO-A-600	10.02	75.6	0.133	6.87
LTO-A-700	12.17	54.4	0.122	6.9
LTO-B-600	8.42	123	0.168	6.15
LTO-B-700	9.78	110	0.162	6.16
LTO-C-700	10.90	68.3	0.078	4.72

[*] The average crystallite size was calculated using the Scherrer equation by averaging the values obtained for the peaks corresponding to the (111), (131), (040), (151), and (404) planes. [**] Pore size distribution was evaluated using the BJH method from the adsorption branch. S_{BET} is specific surface area (BET); V_{pore} is average pore volume; d_{pores} is average pore diameter.
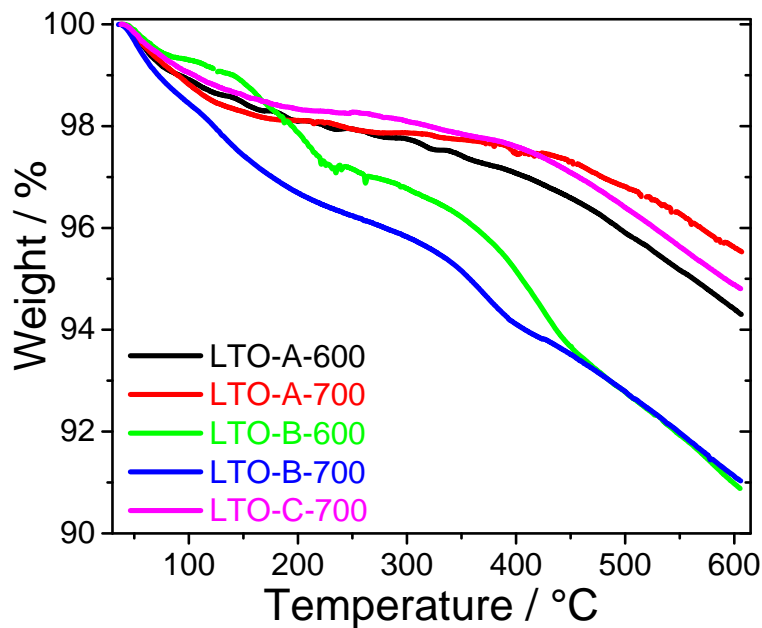
Figure S2: Thermogravimetric analysis (TGA) of carbon-coated mesoporous LTO microspheresThe signal in the temperature range between 25 and 200 °C is attributed to adsorbed water, which amounts to less than 2 wt.%) for all samples except for LTO-B-700 (about 3.4 wt.% loss).[5] The weight loss in the temperature range of 400 to 600 °C corresponds to the degradation of the carbon coating, which amounts to less than 6 wt.% for all samples except for LTO-B-600 and LTO-B-700 that both show about 9 wt.% reduction in mass.
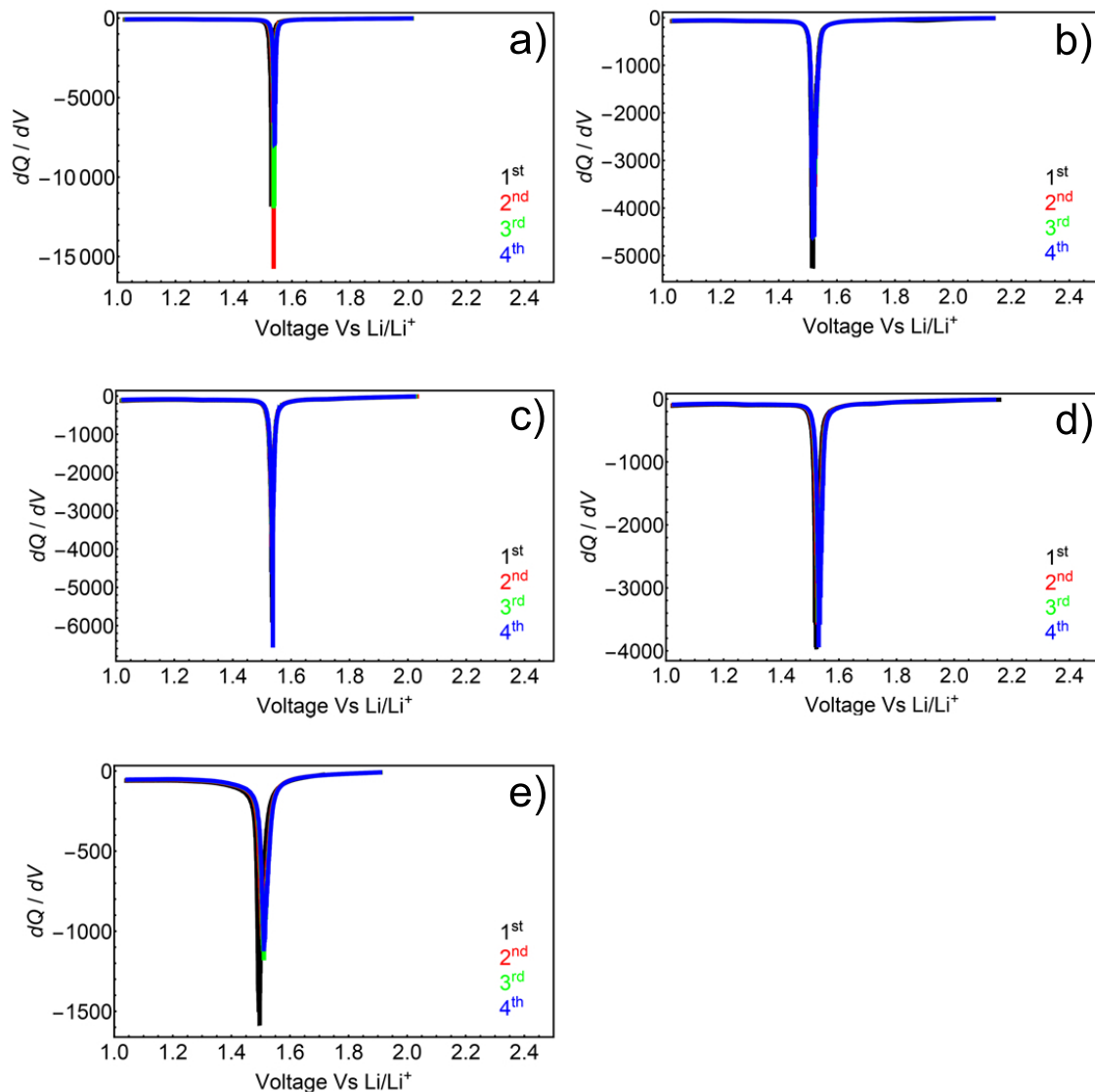
Figure S3: dQ/dV discharge profiles from the first four cycles (0.5 C-rate) of mesoporous LTO-A-600 (a), LTO-A-700 (b), LTO-B-600 (c), LTO-B-700 (d) and LTO-C-700 (e) microspheres. The discharge plateau potentials were found to decrease from approx. 1.54 V to approx. 1.52 V with the increase of crystallite size resulting from increasing annealing temperature.[6,7]
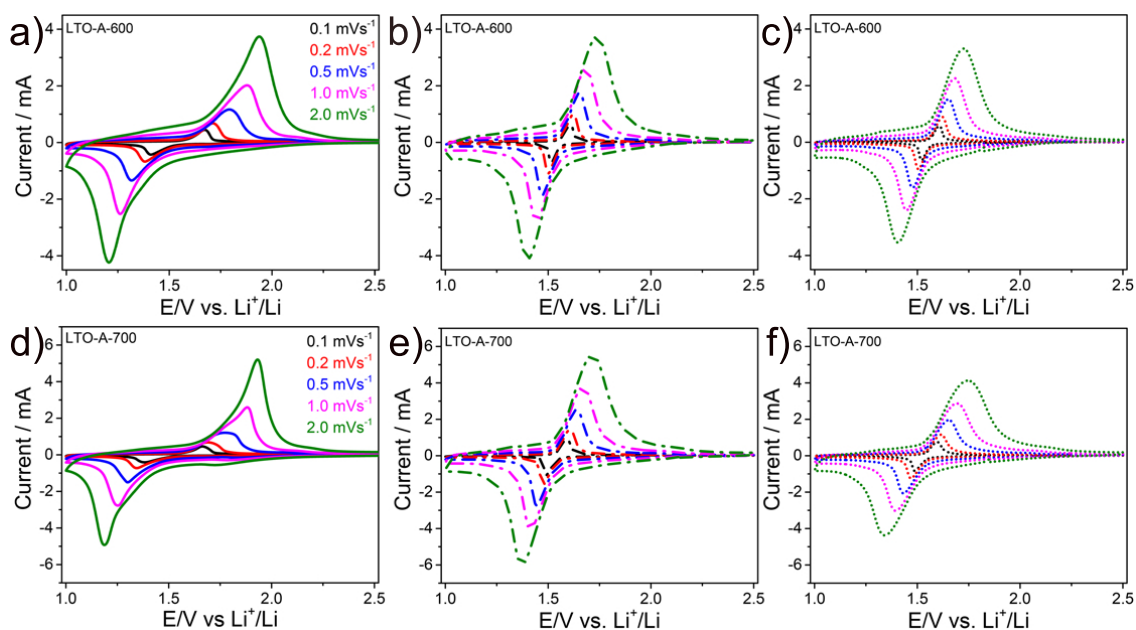
Figure S4: CV profile of the mesoporous LTO-A-600 (top row), and LTO-A-700 microspheres (bottom row), respectively. (a, d) post-assembly; (b, e) post-rate test; (c, f) post-cycle test at a C-rate of 10 for 1000 cycles.
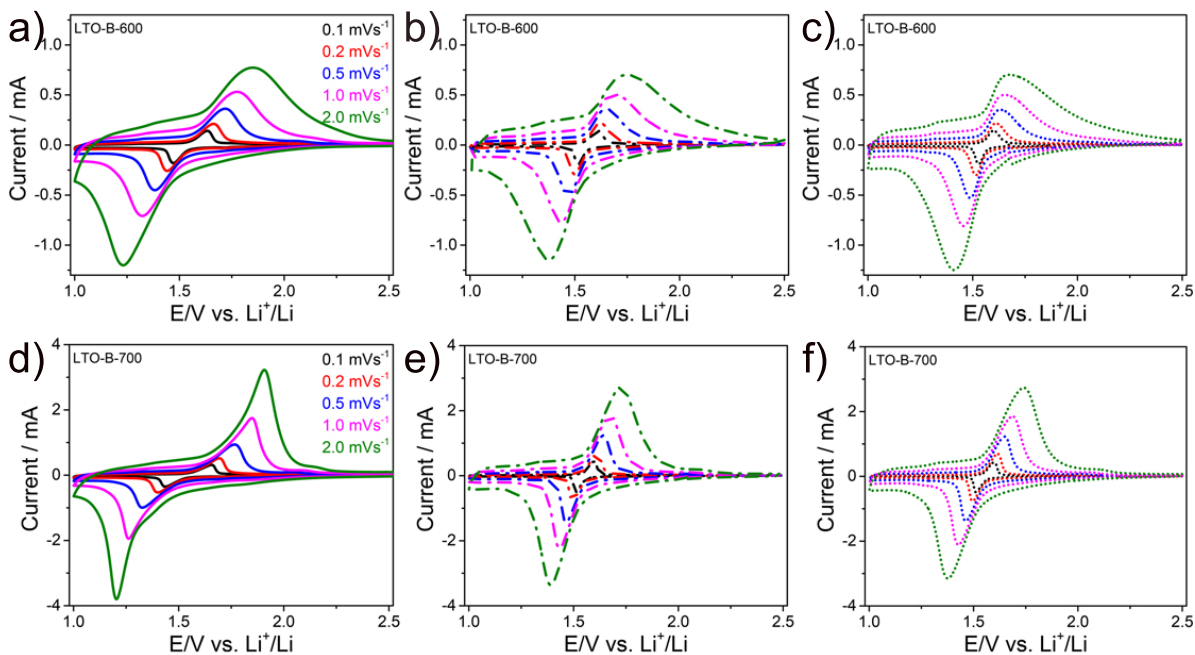

Figure S5: CV profile of the mesoporous LTO-B-600 (top row), and LTO-B-700 microspheres (bottom row), respectively. (a, d) post-assembly; (b, e) post-rate test; (c, f) post-cycle test at a C-rate of 10 for 1000 cycles.
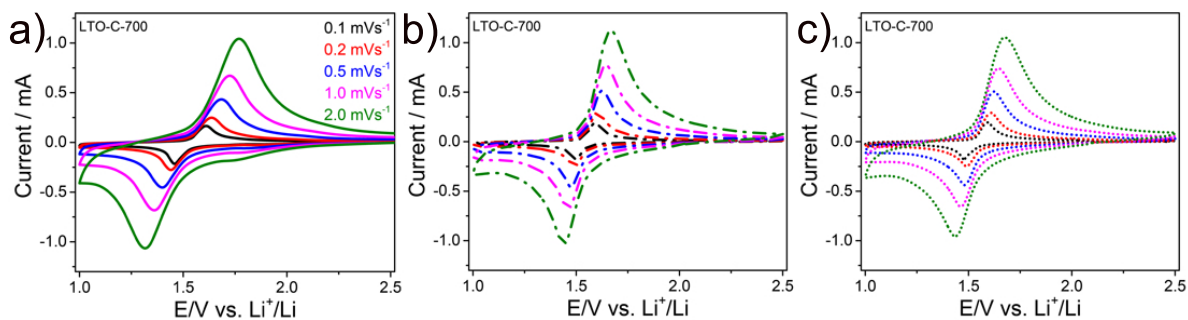
Figure S6: CV profile of the mesoporous LTO-C-700 microspheres. (a) post-assembly; (b) post-rate test; (c) post-cycle test at a C-rate of 10 for 1000 cycles.
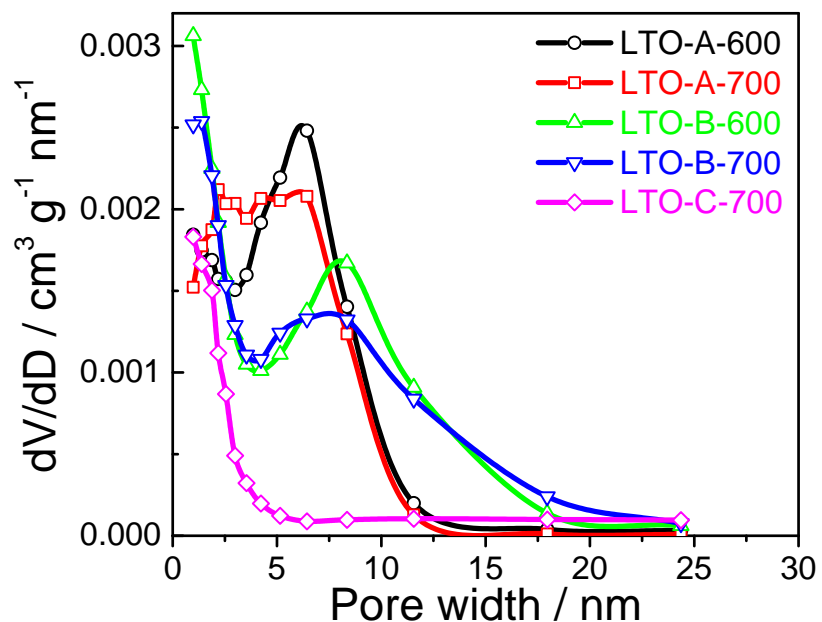

Figure S7: Pore size distribution as determined from the adsorption branch using the BJH method, where the derivative pore volume normalised to the pore-diameter interval, dV/dD, is shown as a function of the pore width.

References

(1) Snyder, M. Q.; DeSisto, W. J.; Tripp, C. P. An infrared study of the surface chemistry of lithium titanate spinel ($Li_4Ti_5O_{12}$). *Applied Surface Science* **2007**, *253*, 9336–9341.

(2) Pasierb, P.; Komornicki, S.; Rokita, M.; Rekas, M. Structural properties of Li_2CO_3-$BaCO_3$ system derived from IR and Raman spectroscopy. *Journal of Molecular Structure* **2001**, *596*, 151–156.

(3) Yue, J.; Suchomski, C.; Brezesinski, T.; Smarsly, B. M. Polymer-Templated Mesoporous $Li_4Ti_5O_{12}$ as a High-Rate and Long-Life Anode Material for Rechargeable Li-Ion Batteries. *ChemNanoMat* **2015**, *1*, 415–421, _eprint: https://onlinelibrary.wiley.com/doi/pdf/10.1002/cnma.201500078.

(4) Gao, Y.; Wang, Z.; Chen, L. Stability of spinel $Li_4Ti_5O_{12}$ in air. *Journal of Power Sources* **2014**, *245*, 684–690.

(5) Zhang, J.; Cai, Y.; Wu, J.; Yao, J. Graphene oxide-confined synthesis of $Li_4Ti_5O_{12}$ microspheres as high-performance anodes for lithium ion batteries. *Electrochimica Acta* **2015**, *165*, 422–429.

(6) Wagemaker, M.; Mulder, F. M. Properties and Promises of Nanosized Insertion Materials for Li-Ion Batteries. *Accounts of Chemical Research* **2013**, *46*, 1206–1215, Publisher: American Chemical Society.

(7) Ganapathy, S.; Wagemaker, M. Nanosize Storage Properties in Spinel $Li_4Ti_5O_{12}$ Explained by Anisotropic Surface Lithium Insertion. *ACS Nano* **2012**, *6*, 8702–8712, Publisher: American Chemical Society.